Journal of Marine Research, 56, 41–74, 1998

A streamtube model of rotating turbidity currents

by P. W. Emms[1]

ABSTRACT

A rotating turbidity current is modeled as a steady tube of sediment-laden water traversing along and down a uniform slope representing the continental shelf. The model includes parameterizations of erosion of sediment from the seabed into the plume, deposition onto the seafloor, bottom friction, and turbulent entrainment of the overlying ambient seawater. The purpose of the work is to study how these parameterizations affect the path the current takes on the slope and to determine criteria which affect the qualitative behavior of the model solutions.

It is found that there are three possible final states to the model. The first is near-geostrophic flow along the slope which is similar to the uniform state found in streamtube models. The second is the catastrophic state which describes an erosive current entraining and depositing a large amount of sediment and traveling downslope much like an avalanche. In the third state the current decelerates and flows along slope whilst depositing its load. The current is extinguished on a length scale $2(aQ_*/v_sK_f r_0)^{1/2}$ from the source where a is the aspect ratio, Q_* is the initial volume flux, v_s is the settling velocity, K_f is a frictional coefficient and r_0 is the deposition rate.

The state the current adopts depends on the initial conditions and model parameters. A linear stability analysis finds that the geostrophic state is always unstable while the catastrophic state is always stable. Thus the model predicts either catastrophic flow down slope or depositional flow along-slope. Given a sufficiently large initial disturbance the current will always ignite. This behavior is illustrated with parameters appropriate to the Kveitehola outflow. However the catastrophic state is unrealistic in that the turbulent energy required to maintain the sediment in suspension can be greater than that available to the current. Consequently a five-equation model is introduced which contains a turbulent kinetic energy equation and a parameterization of interfacial shear stress based on turbulence. With this model the Coriolis force has a much greater impact on the plume's path and the sediment erosion is not so unreasonably large.

1. Introduction

Submerged gravity currents arise on the seabed as a result of a density contrast with the surrounding fluid. This density contrast can arise from a variety of different physical processes such as evaporation, freezing, or water-mass mixing. The subject of this work is the study of a gravity current driven by a suspended sediment. Such a flow is known as a turbidity current. One characteristic feature of a turbidity current is that sediment is not a conserved quantity so that the driving force varies both spatially and temporally.

1. James Rennell Division, Southampton Oceanographic Centre, Empress Dock, Southampton, SO14 3ZH, United Kingdom.

An earthquake, a storm or internal gravity waves may trigger a disturbance of sediment on the seafloor giving rise to a turbidity current: the resulting turbulent flow entrains more sediment which further drives the flow downslope. Often the erosion of the ocean floor is so great that a canyon forms. At a later stage the current slows as the slope diminishes and the plume spreads into a fan with sediment being deposited onto the seabed. A review of submarine fan morphology can be found in Bouma *et al.* (1985). Eventually a characteristic layer of sediment known as a turbidite forms on the seafloor (Piper and Savoye, 1993). Thus, turbidity currents are an important mechanism for nutrient and sediment transfer in the deep ocean. Observation of the events causing turbidite formation in the ocean is difficult. This led a number of investigators to study turbidity currents in the laboratory (Bonnecaze *et al.,* 1993; Huppert *et al.,* 1995; Rimoldi *et al.,* 1996). None of these experimental studies consider the action of the Coriolis force on the path of the plume. This paper presents the derivation and analysis of a mathematical model of a rotating turbidity current.

Much research has concentrated on constructing models of rotating gravity currents which are density driven through temperature and salinity differences. The simplest models consider the steady flow of an inviscid plume which conserves potential vorticity and flows *along* a uniform slope (Griffiths, 1986). From such a simple basic state one can analyze the temporal stability of one and two layer models (Griffiths *et al.,* 1982; Swaters, 1991; Swaters and Flierl, 1991). A more realistic description is the streamtube model formulated by Smith (1973; 1975) which includes parameterizations of bottom friction and entrainment. He found that a steady tube of fluid flows approximately along isobaths in geostrophic balance, and only descended the slope due to bottom friction. Price and Baringer (1994) have recently generalized this model further by allowing for the inclusion of realistic bottom topography and more sophisticated entrainment and spreading laws. This allows the model to be compared to observational data for well-known oceanic outflows such as through the Denmark Straits (Jungclaus and Backhaus, 1994).

A *nonrotating* turbidity current can adopt a number of different states (Pantin, 1979; Parker, 1982; Parker *et al.,* 1986). Parker (1982) characterized these states by looking at steady solutions to a one-dimensional model. He found two uniform solutions: an ignitive and a catastrophic state. The first state is temporally unstable so he used it to determine under what initial conditions a turbidity current would "ignite," that is accelerate downslope much like an avalanche. Once ignited the plume eventually reaches the steady catastrophic state which is temporally stable. The other possibility is that the plume will deposit its load and eventually cease to exist since there is no longer any driving force. Dade *et al.* (1994) have determined the length scale on which such a deposition takes place and have compared their results to turbidite measurements.

Nof (1996) has recently considered a model of the turbidity current arising from the Grand Banks earthquake in 1929. His model studied the effect the Coriolis force and bottom slope had on a blob of dense fluid descending the continental slope. Erosion, deposition of sediment, bottom friction and fluid entrainment were not considered. The mean path was found to a cycloid aligned along isobaths. These inertial oscillations are similar to those found in streamtube models (Emms, 1997) with small values of bottom

friction. For a convex bottom the major axis of the ellipse which the blob follows is aligned along slope whereas for a concave bottom the major axis is aligned downslope. Thus the curvature observed in the path of the blob and the speed decrease as it turned were offered as explanations for the observations of the breakage times in cables on the path of the Grand Banks turbidity current. However turbidite measurements (Clarke *et al.,* 1990) suggest that the Grand Banks turbidity current was eroding and accelerating for at least 100 km from the shelf-break. Consequently it seems important to construct a turbidity current model which allows sediment exchange.

In the following section we present the turbidity current model described in Parker *et al.* (1986) with the addition of rotational effects. The model is then nondimensionalized and the important parameters are identified. In Section 3 we average over a cross-section of tube and arrive at a streamtube model of a turbidity current which includes parameterizations of erosion and deposition. We then find two uniform solutions of this model: one representing geostrophic alongslope flow and one representing catastrophe with the flow downslope. An approximate solution describing the extinction of a depositing current is also given. The model is also solved numerically to illustrate the path the current can take on the slope. This qualitative description uses parameters chosen to represent the Kveitehola outflow. Section 4 details a linear stability analysis which determines under what parameter values and under what initial conditions we would expect to see the possible final states of the model. Section 5 derives an energy equation for the tube and describes how this puts further limitations on the evolution to the catastrophic state. Further extensions to the model are considered in the final section.

2. Model formulation

The model for the turbidity current originates from the shallow water equations for a submerged layer of fluid on a slope at an angle S to the horizontal (see Fig. 1) with axes x along the slope and y down the slope. A derivation of the equations for the nonrotating case can be found in Parker *et al.* (1986). The derivation for the rotating case involves adding the Coriolis force to the Navier-Stokes equations with a sediment transport equation and then carrying out the averaging process over the layer depth. The resulting equations involve the average horizontal velocity $\mathbf{U} = (u, v)$, the layer depth h and the volumetric concentration of sediment in the plume C. For simplicity we suppose the ambient fluid above the sediment-laden plume is nonstratified and motionless and that the sediment in the plume is noncohesive. Conservation of mass, sediment and momentum can be expressed in the form

$$(uh)_x + (vh)_y = w_e, \tag{2.1a}$$

$$(uCh)_x + (vCh)_y = v_s(E_s - C_b), \tag{2.1b}$$

$$(u^2h + \tfrac{1}{2}RgCh^2)_x + (uvh)_y - fvh = -u_*^2, \tag{2.1c}$$

$$(uvh)_x + (v^2h + \tfrac{1}{2}RgCh^2)_y + fuh = -v_*^2 + RgChS. \tag{2.1d}$$

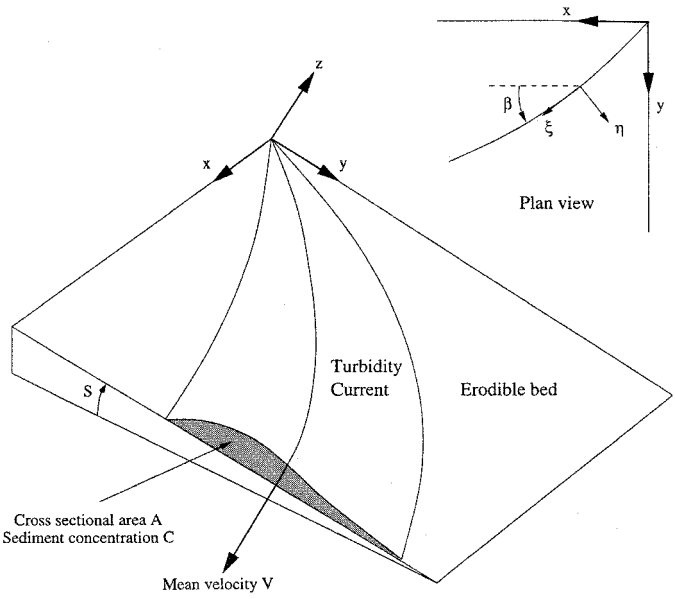

Figure 1. Schematic of a rotating turbidity current spreading down and moving along a uniform slope.

Here w_e is the entrainment velocity of ambient fluid which serves to decrease the concentration of sediment in the plume and thus reduce the driving force $RgChS$. If the settling velocity of sediment is v_s, then we suppose the sediment flux into the plume is $v_s E_s$ and the flux onto the seafloor is $-v_s C_b$. The concentration of sediment very close to the seabed (above a viscous region) is denoted by C_b. The specific gravity of the sediment is R, f is the Coriolis parameter and $\mathbf{u}_* = (u_*, v_*)$ is the shear velocity near the seabed.

In stating (2.1) we have assumed the pressure is hydrostatic, the tube is self-similar in the vertical and that all shape factors are set to one: the details can be found in Parker *et al.* (1986). To make further progress we adopt some parameterizations. The entrainment of ambient fluid is assumed to be proportional to the mean velocity in the layer (Ellison and Turner, 1959):

$$w_e = e_w |\mathbf{U}|. \tag{2.2}$$

The coefficient e_w is often taken as a function of the Richardson number (Turner, 1986). We do not consider such complications here although such a relationship is useful in determining an appropriate value for e_w. Often the Richardson number is large which leads to a small value of e_w. Next we suppose the interfacial shear stress is dominated by the bottom friction and this can be parameterized by a quadratic drag law:

$$(u_*^2, v_*^2) = K_f |\mathbf{U}| \mathbf{U}, \tag{2.3}$$

where K_f is a frictional coefficient. It remains to parameterize the entrainment of sediment E_s and the concentration of sediment near the bottom C_b.

A number of experimental observations lead to a suitable parameterization of E_s. Below some critical value of the shear (called the Shields stress) there is no entrainment of sediment into the plume. As the flow velocity is increased more sediment is entrained until another critical shear stress is reached and thereafter entrainment of sediment remains constant. A dimensionless measure of the strength of the flow often used to parameterize erosion (Akiyama and Fukushima, 1985; Parker *et al.,* 1986; Garcia and Parker, 1993) is

$$Z = R_p^{1/2} |\mathbf{u}_*| / v_s, \tag{2.4}$$

where R_p is the pore Reynolds number defined by

$$R_p = \frac{(RgD_s)^{1/2} D_s}{\nu}, \tag{2.5}$$

D_s is the particle diameter and ν is the kinematic viscosity of clear water. The factor $R_p^{1/2}$ is included to reconcile the experimental observation that finer grain sediment entrains at about the same rate as coarser grain sediment (Garcia and Parker, 1993). We shall adopt the parameterization of Akiyama and Fukushima (1985) who defined

$$E_s = \begin{cases} E_{sm} & Z > Z_m, \\ 3 \times 10^{-12} \times Z^{10} \left(1 - \dfrac{Z_c}{Z}\right) & Z_c < Z < Z_m, \\ 0 & Z < Z_c. \end{cases} \tag{2.6}$$

Akiyama and Fukushima (1985) found experimentally (based on grain diameters in the range 0.06–1.00 mm) that the critical velocity above which erosion took place was $Z_c \sim 5.0$ and the maximum value after which the sediment entrainment became constant at $E_{sm} \sim 0.3$ was $Z_m \sim 13.2$. This parameterization was based on experiments conducted on open channel flows. Recently Garcia and Parker (1993) have found that experiments on submerged gravity currents yield a relationship of the same form as (2.6).

The concentration near the seabed is parameterized by $C_b = r_0 C$ where r_0 is taken for simplicity to be constant. More generally one can take r_0 to be a function of the stream velocity as one would expect a slowly flowing stream to deposit more of its load. However, a constant value of r_0 fits the experimental data just as well as the more complicated functional forms given in Parker *et al.* (1986). Note that Bonnecaze *et al.* (1993) take $r_0 = 1$ in their model for a depositing current.

a. Nondimensionalization

We adopt a velocity scale based on a balance between friction and gravity as in river flow so that $V_* = RgC_* h_* S/K_f$. Here C_* is the volumetric concentration scale in the plume and h_* is the height scale. The concentration can vary considerably depending on the type of

turbidity current; low density turbidity plumes have $C_* \sim 10^{-5}$ whereas mud flow has a concentration $C_* \sim 0.1$ (Stow, 1994). We take a compositional scale based on a balance between erosion and deposition $C_* = E_{sm}/r_0$ which gives a very large concentration scale but is a convenient nondimensionalization. A number of length scales exist in the equations: the deformation radius $(RgC_*h_*)^{1/2}/f$, the topographic length scale U_g/f where U_g is a geostrophic velocity scale, or scales based on the entrainment or sediment transfer. However we shall adopt a scale based on a balance between friction and inertia to yield $L = h_*/K_f$. This provides a scale of the order of kilometers and is a useful benchmark on which to judge the other length scales. Finally we choose a height scale so that the initial nondimensional volume flux is one. Therefore $h_*^2 = aQ_*/V_*$ where a and Q_* are the aspect ratio and initial volume flux, respectively. Thus to summarize the scales are

$$V_* = \left[\frac{aQ_*(RgC_*S)^2}{K_f^2}\right]^{1/5}, \qquad h_* = \left[\frac{a^2Q_*^2K_f}{RgC_*S}\right]^{1/5}, \qquad L = h_*/K_f, \quad C_* = \frac{E_{sm}}{r_0}. \tag{2.7}$$

Under these scalings the dimensional equations (2.1) become

$$(uh)_x + (vh)_y = E|\mathbf{U}|, \tag{2.8a}$$

$$(uCh)_x + (vCh)_y = B\left(\frac{E_s}{E_{sm}} - C\right), \tag{2.8b}$$

$$\left(u^2h + \frac{K_f}{2S}Ch^2\right)_x + (uvh)_y - \frac{vh}{Ro} = -|\mathbf{U}|u, \tag{2.8c}$$

$$(uvh)_x + \left(v^2h + \frac{K_f}{2S}Ch^2\right)_y + \frac{uh}{Ro} = -|\mathbf{U}|v + Ch, \tag{2.8d}$$

where the entrainment and deposition parameters are

$$E = \frac{e_w}{K_f}, \qquad B = \frac{r_0v_s}{K_fV_*}, \tag{2.9}$$

and the Rossby number is $Ro = V_*/fL$. Using a frictional balance to determine V_* and L means the Rossby number will be large. This does not necessarily mean the Coriolis force is unimportant because there are other length scales which might be more appropriate to particular model solutions. The system of equations (2.1) has been reduced to a system depending on four parameters: E, B, Ro and the erosional capacity α defined by

$$\alpha = \frac{\sqrt{|R_pK_f}V_*}{v_s}, \tag{2.10}$$

so that $Z = \alpha V$ in nondimensional variables and the parameterization of erosion becomes $E_s = E_s(\alpha V)$. The choice of a large velocity scale means that α will be a large parameter.

Fine sediment tends to have a larger value of α which means at a fixed velocity more sediment is entrained into the tube. The case of a conservative gravity current can be recovered by setting $B = 0$. In the absence of friction a conservative density current flows along isobaths in geostrophic balance (Griffiths, 1986). Ageostrophic initial conditions lead to oscillations about this mean path (Nof, 1996).

3. The streamtube approximation

To make further progress we adopt the streamtube approximation of Smith (1975) and Killworth (1977). First we suppose the position of the tube on the slope can be described by a centerline $x = X_p$, $y = Y_p$ where

$$\frac{dX_p}{d\xi} = \cos\beta, \qquad \frac{dY_p}{d\xi} = \sin\beta, \tag{3.1}$$

where β is the angle the centerline makes with the x-axis. Next we transform the nondimensional equations (2.8) using streamtube coordinates ξ, η (see Fig. 1) given by

$$x = X_p - \eta\sin\beta, \tag{3.2a}$$

$$y = Y_p + \eta\cos\beta. \tag{3.2b}$$

It is simple to show from (3.2) that the scale factor perpendicular to the centerline is one whilst the scale factor along the centerline is

$$H = 1 - \eta\frac{d\beta}{d\xi}, \tag{3.3}$$

and β_ξ is the curvature of the centerline.

Using the identities for curvilinear coordinate systems (Batchelor, 1967, Appendix 2) we can write the nondimensional equations in the form

$$(\mu h)_\xi + (H\nu h)_\eta = EH|\mathbf{U}|, \tag{3.4a}$$

$$(\mu Ch)_\xi + (H\nu Ch)_\eta = BH\left(\frac{E_s}{E_{sm}} - C\right), \tag{3.4b}$$

$$h(\mu\mu_\xi + H\nu\mu_\eta) + \frac{K_f}{2S}(Ch^2)_\xi - \frac{H\nu h}{Ro} = -H(E+1)|\mathbf{U}|\mu + HCh\sin\beta, \tag{3.4c}$$

$$h(\mu\nu_\xi + \nu(H\nu)_\eta + \mu^2\beta_\xi) + \frac{HK_f}{2S}(Ch^2)_\eta + \frac{H\mu h}{Ro} = -H(E+1)|\mathbf{U}|\nu + HCh\cos\beta, \tag{3.4d}$$

where μ and ν are the components of velocity along and perpendicular to the center line. Eqs. (3.4c) and (3.4d) express conservation of momentum along and across the tube respectively.

Inherent in this transformation is the assumption that the curvature of the center line is sufficiently small so that the transformation is well defined. One can avoid this requirement by using the streamfunction as a transverse coordinate (Emms, 1997) at the expense of only considering non-entraining flow.

We must make some additional assumptions to arrive at a streamtube model. Firstly we suppose the along-tube velocity is much larger than the across-tube velocity, that is $\mu = V \gg \nu$. Next we suppose that the velocity V and concentration C are only functions of the alongstream coordinate ξ. Thirdly we neglect the pressure terms due to changes in height of the tube above the slope (the third and fourth terms in (3.4c) and (3.4d), respectively). Emms (1997) has considered the relaxation of this last assumption in the context of gravity currents arising from temperature or salinity contrasts. Under streamtube approximations it is consistent to include the along-tube term and then the equations are similar to problems in hydraulics or river flow. The Froude number of the tube is a critical parameter which determines the types of possible solutions. However the model doesn't successfully predict observations so that Emms concluded one must consider a two dimensional tube model if these extra pressure terms are to be included.

Finally we suppose the curvature of the centerline is small so that $H \sim 1$. These approximations reduce (3.4) to

$$(Vh)_\xi = EV, \tag{3.5a}$$

$$(VCh)_\xi = B\left(\frac{E_s}{E_{sm}} - C\right), \tag{3.5b}$$

$$hVV_\xi = -(E+1)V^2 + Ch\sin\beta, \tag{3.5c}$$

$$hV^2\beta_\xi + Vh/Ro = Ch\cos\beta. \tag{3.5d}$$

To complete the model we integrate over a cross-section of tube to give the streamtube equations:

$$(AV)_\xi = EwV, \tag{3.6a}$$

$$(AVC)_\xi = Bw\left(\frac{E_s}{E_{sm}} - C\right), \tag{3.6b}$$

$$(AV^2)_\xi = -wV^2 + AC\sin\beta, \tag{3.6c}$$

$$V^2\beta_\xi = C\cos\beta - V/Ro, \tag{3.6d}$$

where w is the width and A is the cross-sectional area of the tube.

To close the model we must specify a relation for the tube width w, which is a consequence of ignoring gradients across the tube. For the original streamtube model Killworth (1977) assumed the plume was self-similar. A more recent model (Price and Baringer, 1994) has supposed the change in width is proportional to the Ekman number

since bottom friction determines how the tube spreads. Both parameterizations have been successfully compared with observations, so for simplicity we suppose the tube is self-similar, that is we set

$$w = h = A^{1/2}, \tag{3.7}$$

by our choice of scaling. Consequently we finally obtain the streamtube model equations for a turbidity current:

$$(AV)_\xi = EA^{1/2}V, \tag{3.8a}$$

$$(AVC)_\xi = BA^{1/2}\left(\frac{E_s}{E_{sm}} - C\right), \tag{3.8b}$$

$$(AV^2)_\xi = -A^{1/2}V^2 + AC\sin\beta, \tag{3.8c}$$

$$V^2\beta_\xi = C\cos\beta - V/Ro. \tag{3.8d}$$

By way of analogy with Parker *et al.* (1986) we call (3.8) the four-equation model. It corresponds to their three-equation model: the extra equation is the across-stream momentum balance (3.8d).

a. Typical parameter values

Due to the difficulties in obtaining observational data for a turbidity current in the deep ocean ascribing values to the parameters identified in the model is at best speculative. Recently Fohrmann *et al.* (1997) presented a numerical simulation of the Kveitehola outflow which flows from the Barent Sea into the Greenland Sea. We shall use their estimates for that outflow as a guide to appropriate parameter values for the model. To integrate (3.8) we also specify values for the initial conditions at the tube source (denoted by a subscript s): A_s, V_s, C_s and β_s.

From turbidite records Fohrmann *et al.* inferred that the Kveitehola outflow occurred as a result of a surge of sediment-laden fluid of width 5 km and height 20 m traveling at a velocity of 0.15 m s^{-1}. This gives an initial flux of 1.5×10^4 m^{-3} s^{-1} through the Kveitehola valley. Fohrmann also assumed the initial volumetric concentration of particles was 3.77×10^{-5} and that the current contained two grain sizes: a medium grain size $D_s =$ 20 μm and a coarse grain size $D_s = 63$ μm. For simplicity we shall only consider a model containing one grain size. Tubes containing medium and coarse sediments will be considered separately. The density of the particles is taken to be that of quartz so that the specific gravity is $R = 1.65$. Since both currents have the same volumetric concentration the coarse grain current contains fewer particles initially than does the medium grain current. The initial Richardson number of the tube is $Ri = RCgh/V^2 \sim 0.54$ and if we follow Parker *et al.* (1986) then $e_w = 0.00153/(0.0204 + Ri) \sim 2.7 \times 10^{-3}$. The frictional coefficient is set at $K_f = 10^{-3}$ and the depositional constant $r_0 = 1.6$ to fit the experimental results shown in Parker *et al.* (1986). As we are interested in the qualitative features of the

Table 1. Approximate parameters and initial values for the Kveitehola outflow.

Scales		
Downslope velocity scale V^* (m s^{-1})	11.0	
Cross-sectional Area scale A^* (m^2)	1.37×10^3	
Length scale L (km)	2.34	
Volumetric concentration scale C^*	0.188	
Parameters		
Coriolis parameter f (s^{-1})	1.40×10^{-4}	
Slope S	1.7×10^{-2}	
Frictional coefficient K_f	10^{-3}	
Entrainment constant e_w	2.7×10^{-3}	
Aspect ratio a	4.0×10^{-3}	
Entrainment parameter E	2.7	
Rossby number Ro	33.5	
Silt	Medium	Coarse
Particle size D_s	20 μm	63 μm
Pore Reynolds number R_p	0.20	1.12
Settling velocity v_s (m s^{-1})	2.00×10^{-4}	1.98×10^{-3}
Deposition rate B	2.91×10^{-2}	0.29
Erosional capacity α	7.77×10^2	1.85×10^2
Initial values		
Cross-sectional area A_s	73.2	
Along-tube Velocity V_s	1.37×10^{-2}	
Volumetric concentration C_s	2.01×10^{-4}	
Angle to x-axis β_s	$\pi/2$	
Turbulence K_s	1.87×10^{-4}	
Five-equation model		
Shear stress coefficient δ	100.0	
Friction k	5.88×10^{-2}	
Silt	Medium	Coarse
Bagnold number G	1.07×10^{-3}	1.06×10^{-2}

model we only consider a uniform slope and so set $S = 1.7 \times 10^{-2}$ which represents an average value. The tube is started pointing downslope which means $\beta_s = \pi/2$. Finally the settling velocity v_s is calculated from Stokes law for the drag on a sphere (Batchelor, 1967):

$$v_s = \frac{gRD_s^2}{18\nu}. \tag{3.9}$$

From these values we can calculate appropriate parameter and initial values and these are shown in Table 1.

b. Uniform solutions

Uniform solutions of (3.8) are those which have no alongstream (ξ) variation. These exist providing there is no entrainment of ambient fluid $E = 0$ which implies the volume

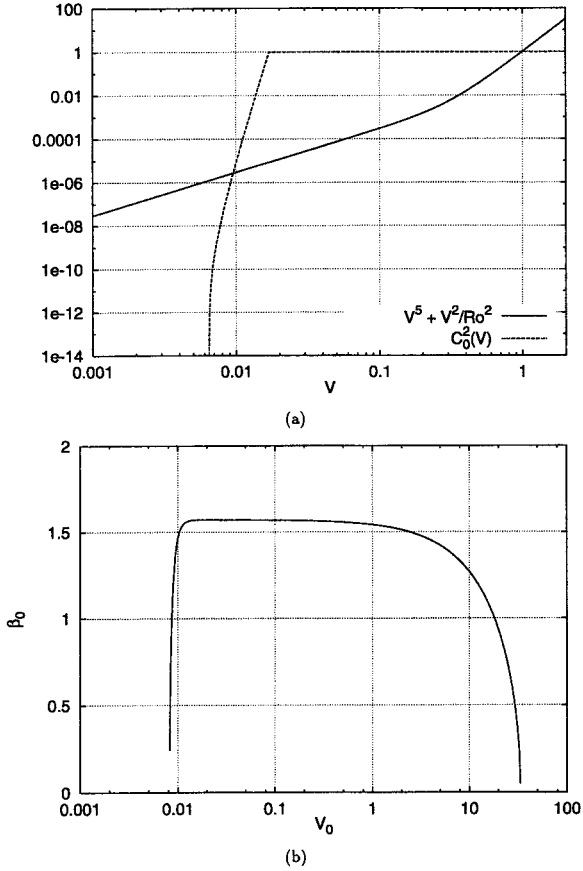

Figure 2. Uniform solutions to the streamtube equations for a medium silt. In (a) the intersection of the two curves gives two uniform solutions. (b) shows that one of these solutions is primarily alongslope while the other is downslope.

flux $Q = AV = 1$ from our choice of scaling. Uniform solutions are therefore given by

$$C_0 = E_s(\alpha V_0)/E_{sm}, \tag{3.10a}$$

$$\cos\beta_0 = \frac{V_0}{RoC_0}, \tag{3.10b}$$

$$V_0^5 + \frac{V_0^2}{Ro^2} - C_0^2 = 0, \tag{3.10c}$$

where we have used a subscript 0 to denote a uniform solution.

Using the values given in Table 1 for a medium slit we plot $V^5 + V^2/Ro^2$ and C_0^2 as functions of V in Figure 2a. The intersection of the two curves gives two uniform solutions and the numerical values are shown in Table 2. Figure 2b shows the angle β_0 as a function of V_0.

Table 2. Uniform solutions to the four and five-equation models with parameters appropriate for a medium silt.

Four-equation model	Geostrophy	Catastrophe
V_0	8.22×10^{-3}	1.00
C_0	2.45×10^{-4}	1.00
β_0	2.50×10^{-2}	1.54
Five-equation model	Geostrophy	Catastrophe
K_0	1.03×10^{-4}	1.00
V_0	0.12	1.00
C_0	3.44×10^{-3}	1.00
β_0	1.02×10^{-2}	1.54

The left-most of these solutions corresponds to the ignitive state (Parker, 1982). Parker found that the ignitive state was temporally unstable and so he used it as a criterion to determine under what initial conditions a turbidity current would ignite. The state also corresponds to the alongslope flow one finds in streamtube models (Smith, 1973): the velocity is approximately geostrophic and the angle β is small. We expect this geostrophic state to be nearly always temporally unstable (Griffiths *et al.,* 1982). The force balance across the tube is between the Coriolis force and the component of gravity downslope (the second and third terms in (3.10c)). The solution is approximately equal to the flow in a tube with no bottom stress:

$$V_0 = RoC_0 = \frac{RoE_s(\alpha V_0)}{E_{sm}}, \qquad \beta_0 = 0. \tag{3.11}$$

The right-most solution is equivalent to the catastrophic state described in Parker (1982). The flow velocity is large: the tube is entraining sediment at the maximum rate E_{sm} which means the sediment load is large and so consequently is the driving force. The corresponding value of β_0 is about $\pi/2$ so that the flow is downslope with the friction balancing the component of gravity (the first and third terms in (3.10c)). Thus approximately the catastrophic state is given by

$$V_0 \sim C_0 \sim 1, \qquad \cos\beta_0 \sim \frac{1}{Ro}, \tag{3.12}$$

which is valid for $Ro \gg 1$ corresponding to small rotation rates. This also reveals the reason for the choice of nondimensionalization. Notice from (3.12) that as Ro decreases the tube turns to flow alongslope. For about $Ro < 1$ or equivalently

$$K_f < \left[\frac{f^5 Q_* a}{(RgC_* S)^3}\right]^{1/2} \tag{3.13}$$

there is no catastrophic solution: the body force has reached its maximum value and there is nothing to balance the Coriolis force. For the values in Table 1 this condition is $K_f < 1.5 \times 10^{-7}$. Thus only at extremely small frictional values does the Coriolis force have any

influence on the catastrophic state. Realistic values of the Rossby number are large so that the Coriolis force has little impact on catastrophe.

Figure 2a and (3.10c) also indicate that for

$$Ro < \frac{\alpha^3 Z_m^2}{\alpha^5 - Z_m^5}, \tag{3.14}$$

there are no uniform solutions at all. In this case the tube slows rapidly and deposits its load.

c. Some approximate solutions

In the ocean the tube may not reach its uniform catastrophic state. Either it could cease to erode more sediment from the ocean floor or as discussed in Section 5 the turbulence in the plume could die out and the sediment deposit. Thus it is useful to have an approximate form of solution on the way to the catastrophe. If we balance friction and gravity alongstream and Coriolis and gravity across-stream then

$$V \sim C^{2/5}, \qquad V \sim RoC\beta^*, \tag{3.15}$$

where we have assumed $\beta^* = \pi/2 - \beta$ is small. Next we balance inertia and erosion in the compositional equation (3.8b) and suppose we have reached maximum erosion E_{sm} so that

$$C_\xi \sim \frac{B}{C^{1/5}}. \tag{3.16}$$

Integrating and applying the initial conditions then gives an approximate solution for a strongly erosive current:

$$C \sim \left(\frac{6B\xi}{5} + C_s^{6/5}\right)^{5/6}, \quad V \sim \left(\frac{6B\xi}{5} + C_s^{6/5}\right)^{1/3}, \quad \beta^* \sim \frac{1}{Ro}\left(\frac{6B\xi}{5} + C_s^{6/5}\right)^{-1/2}. \tag{3.17}$$

None of the solutions described so far considers the case of a tube gradually depositing its load and eroding very little sediment. In this case the entrainment is small so that the volume flux $Q = AV \sim 1$. We also expect the dominant alongstream balance to be between inertia and friction since the sediment load is small giving a small gravitational term in (3.8c). Integrating once yields the alongstream velocity as

$$V \sim \frac{V_s}{(\tfrac{1}{2}V_s^{1/2}\xi + 1)^2}, \tag{3.18}$$

using the initial conditions at the source. Next we balance the rate of change of sediment flux and the deposition term in (3.8b) and then integrate to obtain

$$C \sim C_s \exp\left[-\frac{B}{V_s^{1/2}}\left(\frac{V_s^{1/2}\xi^2}{4} + \xi\right)\right]. \tag{3.19}$$

Thus the plume is extinguished at a distance $\xi = 2/B^{1/2}$ from the source. Reverting to dimensional variables this extinction scale becomes

$$\xi_D = 2\left(\frac{aQ_*}{r_0 v_s K_f}\right)^{1/2}. \tag{3.20}$$

Consequently a large aspect ratio or volume flux increases the extinction scale whereas large deposition rates, settling velocities, or frictional coefficients all decrease ξ_D. In the across-stream momentum equation (3.8d) the body force decreases exponentially and so the dominant balance is between inertia and the Coriolis force. Integrating once gives

$$\beta \sim \frac{\pi}{2} + \frac{2}{3RoV_s^{3/2}}\left(1 - \left(\frac{V_s^{1/2}\xi}{2} + 1\right)^3\right). \tag{3.21}$$

As $\xi \to \infty$, $\beta \to -\infty$ so that the centerline circles clockwise on the slope. Since Q is constant and V is decreasing to zero, the cross-sectional area A increases rapidly and plume spreads out as it deposits. A large Coriolis force corresponds to a small value of Ro which leads to rapid turning.

d. Example model solutions: the Kveitehola Outflow

Three numerical solutions are shown in Figures 3, 4, 5. The first set of graphs shows an entraining tube containing medium silt eroding a large amount of sediment initially and moving downslope toward catastrophe. As water is entrained so the concentration of sediment decreases which decreases the body force so the tube turns slightly to the right looking downstream. To isolate the physical processes and examine the uniform states we shall henceforth only consider a nonentraining current. The second set of graphs shows the evolution to the catastrophic state with parameters appropriate for a medium silt $D_m =$ 20 μm. The third set of graphs is for a coarse silt ($D_m = 63$ μm), and shows the plume depositing its load a finite distance from the source. Once the load is deposited the plume effectively ceases to exist because the interstitial water is the same density as the ambient water.

Superimposed on the plots in Figure 4 is the approximate solution given by (3.17). The agreement is fairly good which indicates the current is strongly erosive. Further downstream the current deposits more sediment and tends toward its equilibrium state. Figure 4a shows that at about 23 km downstream of the source (the length scale is about 2.3 km) the velocity in the tube has grown to nearly its uniform value ($V = 1$) of 11 m s^{-1} which is not inconsistent with reports of speeds of turbidity currents downslope. Figure 4b indicates the volumetric concentration of sediment in the plume has grown by three orders of magnitude. Figure 4d shows the path the tube takes down the slope. The aspect ratio of the graph somewhat distorts the fact that the tube is traveling almost straight down the slope as can be seen from the graph of β in Figure 4c.

Figure 5 for a coarse slit includes the approximate relations (3.18)–(3.21) for a depositing current. There is reasonable agreement, verifying the balances that we assumed.

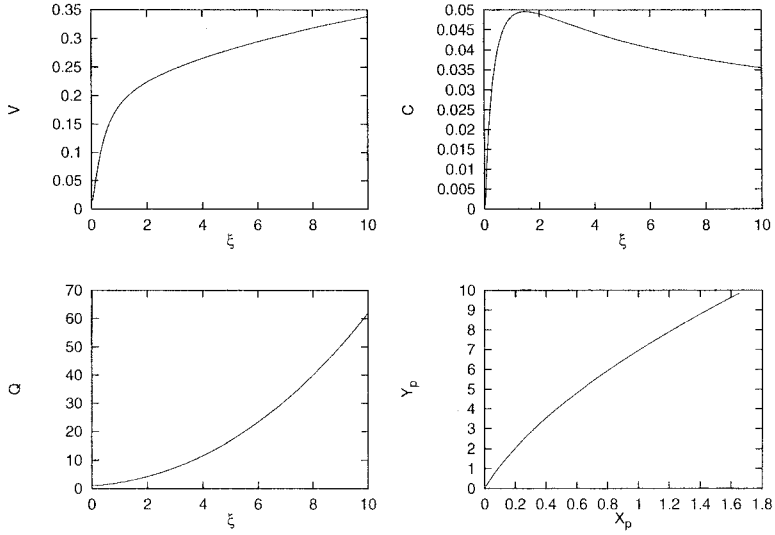

Figure 3. An entraining turbidity current containing medium silt with parameters appropriate to the Kveitehola outflow. The alongstream velocity is V, the volumetric concentration is C, the volume flux is Q and the position on the slope is (X_p, Y_p).

In Figure 5a the numerical solution initially erodes but thereafter agreement with the approximate solution is good. Figure 5b for the plume concentration shows that the current is extinguished at about 7 km downstream (the length scale is about 2.3 km). The plume turns rapidly under the Coriolis force as it slows and deposits sediment. From Figure 5d we see that the plume starts traveling up slope at about $X_p = 0.6$, $Y_p = 0.6$ and it soon crosses itself (since A is large). This invalidates the transformation to streamwise coordinates but it does seem reasonable to suppose that the current will deposit soon thereafter. The circling is caused by the Coriolis force which is still comparatively large compared to the force gravity exerts on the plume. Different initial conditions can lead to a much more rapid extinction of the plume so that this circling is not observed and the plume appears to disappear at a point.

Thus the current can be characterized according to whether it deposits, travels alongslope in geostrophic balance, or travels downslope towards the catastrophic state. These possibilities are summarized in Figure 6. The numerical simulation of Fohrmann *et al.* (1997) exhibits the general behavior of the streamtube model. A large slope leads to vigorous entrainment of sediment and flow downslope, while a more gentle slope leads to deposition and the flow turns to the right.

4. Linear stability analysis of the uniform states

The state the tube finally adopts is determined by both the initial conditions and the parameters one specifies in the model. A linear stability analysis determines whether there are initial conditions which give rise to a particular uniform state. A state is spatially

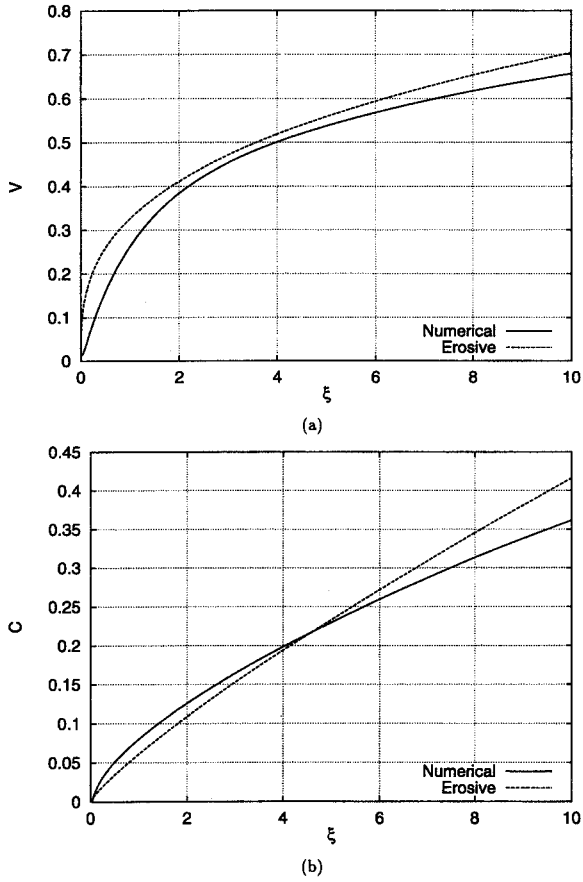

Figure 4. A nonentraining turbidity current containing medium silt with parameters appropriate to the Kveitehola outflow. The dashed lines show the approximate solution for a strongly erosive current (3.17). In (d) the aspect ratio distorts the fact that the tube is traveling predominantly downslope.

stable if there are some initial conditions which yield a tube which evolves to the uniform state.

Physically one expects the catastrophic state to be stable since a large enough initial disturbance should cause ignition. It is not so clear for the geostrophic state. Deviation of the tube downslope should increase the fluid velocity which in turn increases the erosion of sediment and thus increases the component of gravity down slope. However the increase in flow also increases the Coriolis force which would tend to turn the tube back to alongslope flow. Thus the stability of the alongslope state depends on how much larger the body force on the plume increases over the Coriolis force.

We begin by perturbing the uniform state (C_0, V_0, β_0). For uniform solutions to exist

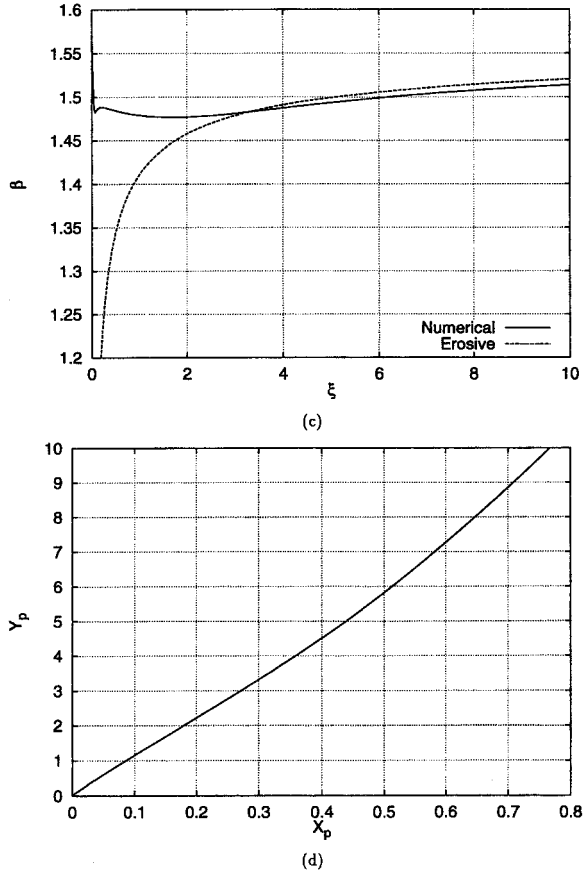

Figure 4 (Continued)

there can be no entrainment so we set $E = 0$ and expand

$$C = C_0 + C', \tag{4.1a}$$

$$V = V_0 + V', \tag{4.1b}$$

$$\beta = \beta_0 + \beta'. \tag{4.1c}$$

Substituting into (3.8) and dropping the primes yields the linearized equations

$$V_0^{1/2} C_\xi = B\left(\frac{\alpha V E_s'(\alpha V_0)}{E_{sm}} - C\right), \tag{4.2a}$$

$$V_0 V_\xi = C \sin\beta_0 + \beta C_0 \cos\beta_0 - \tfrac{5}{2} V_0^{3/2} V, \tag{4.2b}$$

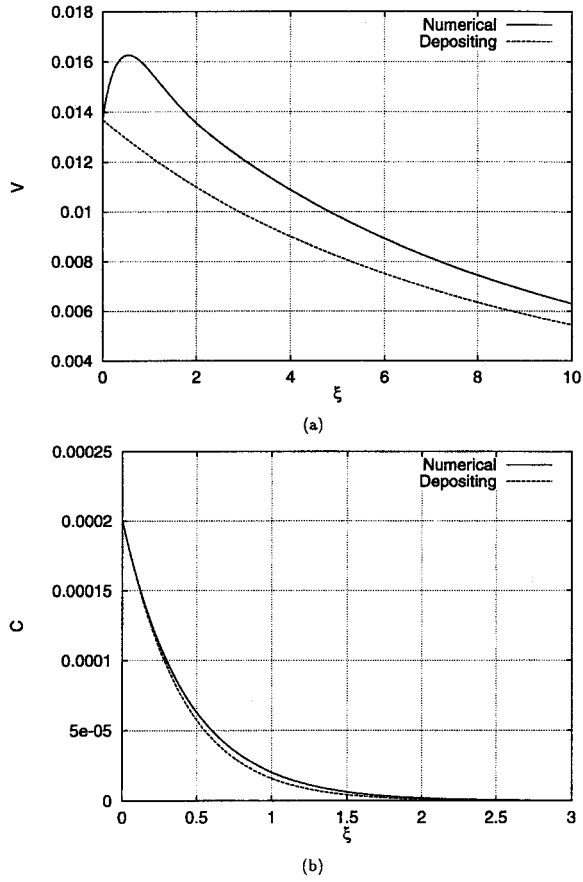

Figure 5. A nonentraining turbidity current containing coarse silt. The dashed lines show the approximate solution for a depositing current (3.18)–(3.21).

$$V_0^2\beta_\xi = C\cos\beta_0 - \beta C_0 \sin\beta_0 - \frac{V}{Ro}. \tag{4.2c}$$

This set of equations has solutions of the form $C = C\exp(\lambda\xi)$ etc., which on substituting into (4.2) gives a linear system

$$\mathscr{L}\mathbf{u} = 0, \tag{4.3}$$

where $\mathbf{u} = (C, V, \beta)^T$ and the matrix $\mathscr{L}$ is

$$\begin{pmatrix} \lambda V_0^{1/2} + B & -\dfrac{\alpha B E_s'(\alpha V_0)}{E_{sm}} & 0 \\ -\sin\beta_0 & \lambda V_0 + \tfrac{5}{2}V_0^{3/2} & -C_0\cos\beta_0 \\ -\cos\beta_0 & 1 & \lambda V_0^2 + C_0\sin\beta_0 \end{pmatrix}. \tag{4.4}$$

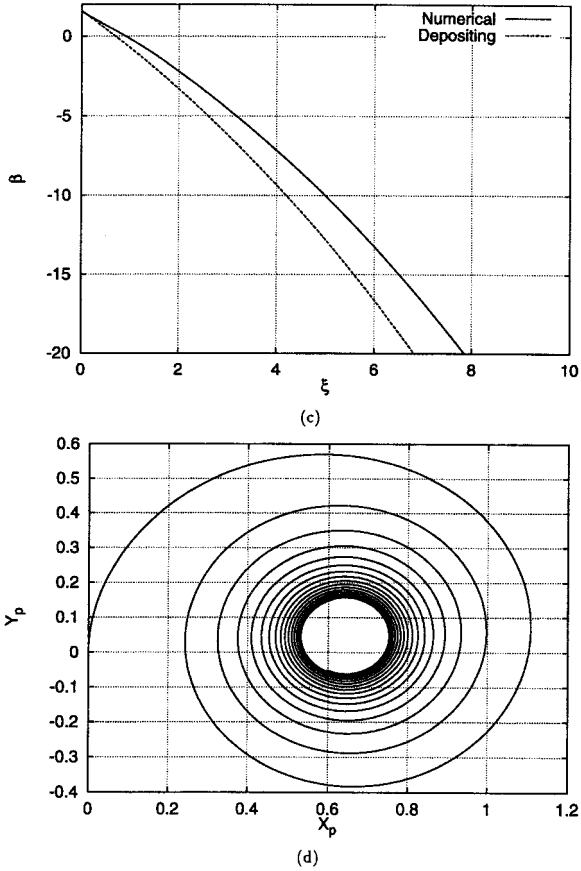

Figure 5 (Continued)

Eq. (4.3) has nontrivial solutions providing det ($\mathscr{L}$) = 0 which yields the following cubic equation for λ

$$V_0^{5/2}\lambda^3 + (BV_0^2 + \tfrac{7}{2}V_0^3)\lambda^2 + \left(\frac{7}{2}BV_0^{5/2} - BNV_0^{7/2} + \frac{5}{2}V_0^{7/2} + \frac{V_0^{1/2}}{Ro^2}\right)\lambda + B\left(\frac{5}{2}V_0^3 + \frac{1}{Ro^2}\right) - BN\left(V_0^4 + \frac{V_0}{Ro^2}\right) = 0. \tag{4.5}$$

Here we have introduced the notation

$$N = \frac{\alpha E_s'(\alpha V_0)}{E_s(\alpha V_0)}, \tag{4.6}$$

and the uniform solution $V_0 = V_0(Ro, \alpha)$ is one of the roots of (3.10c).

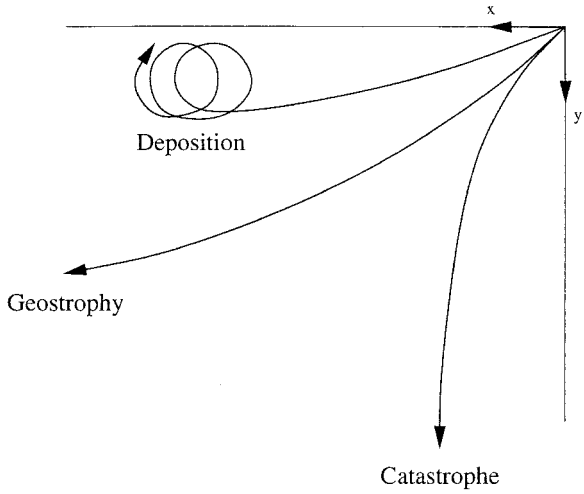

Figure 6. A qualitative description of the possible solutions of the turbidity current model.

The Routh Hurwitz criterion states that the roots of a cubic of the form

$$\lambda^3 + \mathscr{A}\lambda^2 + \mathscr{B}\lambda + \mathscr{C} = 0, \tag{4.7}$$

have negative real part if and only if $\mathscr{A} > 0$, $\mathscr{C} > 0$ and $\mathscr{A}\mathscr{B} > \mathscr{C}$. These are therefore the conditions for stability of a uniform state V_0. Expressions for $\mathscr{A}$, $\mathscr{B}$, $\mathscr{C}$ can be obtained by suitably rearranging (4.5) to give

$$\mathscr{A} = \frac{7\!/\!_2 V_0 + B}{V_0^{1/2}}, \tag{4.8a}$$

$$\mathscr{B} = \frac{7\!/\!_2 BV_0^2 - BNV_0^3 + 5\!/\!_2 V_0^3 + Ro^{-2}}{V_0^2}, \tag{4.8b}$$

$$\mathscr{C} = \frac{B(5\!/\!_2 V_0^3 + Ro^{-2}) - NV_0(V_0^3 + Ro^{-2})}{V_0^{5/2}}. \tag{4.8c}$$

Consequently $\mathscr{A}$ is always positive for all uniform states since B and V_0 are positive.

After some manipulation we find

$$\mathscr{A}\mathscr{B} - \mathscr{C} = \frac{1}{V_0^{3/2}} \cdot \left[\frac{7}{4}\left(7BV_0^2 + 5V_0^3 + \frac{2}{Ro^2} + 2B^2V_0\right) + BN\left(\frac{1}{Ro^2} - \frac{5}{2}V_0^3 - BV_0^2\right)\right]. \tag{4.9}$$

Now since the catastrophic state occurs at the maximum erosion rate E_{sm} it follows that $N = 0$. Thus $\mathscr{A}\mathscr{B} - \mathscr{C}$ and $\mathscr{C}$ are always positive and so the catastrophic uniform state is always stable.

With the aid of the parameterization (2.6) N can be written

$$N = \frac{\alpha}{Z_0}\left(\frac{10Z_0 - 9Z_{0c}}{Z_0 - Z_{0c}}\right), \tag{4.10}$$

for $Z_c < Z < Z_m$, which further reduces the expression for $\mathscr{C}$ to

$$\mathscr{C} = \frac{B}{Ro^2 V_0^{5/2}}\left(\frac{8Z_{0c} - 9Z_0 + \tfrac{1}{2}Ro^2 V_0^3(13Z_{0c} - 15Z_0)}{Z_0 - Z_{0c}}\right). \tag{4.11}$$

Thus for $Z_0 > Z_{0c}$ as must be the case for a geostrophic solution, $\mathscr{C} < 0$. Consequently the uniform geostrophic state is always unstable.

To determine what initial conditions lead to deposition or catastrophe we could look at phase space as did Parker (1982). For a nonrotating plume phase space is primarily two dimensional (ignoring entrainment) whereas for a rotating plume it is three dimensional (V, C, β) and consequently more difficult to visualize. Parker split the domains of dependence up with an autogeneration line (AGL). On one side of the line initial conditions lead to ignition and on the other initial conditions lead to deposition. For a rotating plume this separation requires we calculate a surface. We are concerned here with a qualitative understanding of turbidity currents and we are not seeking to obtain a quantitative prediction of ignition. One should also note that the convergence lines calculated by Parker correspond to the approximate relations we calculated for catastrophe and deposition.

5. A five-equation model

Parker *et al.* (1986) have shown the catastrophic state is unrealistic in that the energy required to maintain the sediment in suspension is greater than that available to the plume. Since the Coriolis force is usually a small part of the momentum balance in this state we expect their results to carry over to our rotating current model. Following their work we therefore construct a slightly more complicated streamtube model which includes a turbulent kinetic energy equation.

The dimensional energy equation for the mean velocity is found by taking the scalar product of **U** and the momentum equations (2.1c,d). After some simplification we find

$$\frac{\partial}{\partial x}\frac{1}{2}uh(u^2 + v^2) + \frac{\partial}{\partial y}\frac{1}{2}vh(u^2 + v^2) = RgChvS - Ph - \frac{1}{2}Rg\left(u\frac{\partial Ch^2}{\partial x} + v\frac{\partial Ch^2}{\partial y}\right), \tag{5.1}$$

where P is rate of transfer of kinetic energy from the mean flow to the turbulence:

$$Ph = \tfrac{1}{2}w_e(u^2 + v^2) + uu_*^2 + vv_*^2. \tag{5.2}$$

In (5.2) the first term represents the loss of mean energy due to entrainment whilst the second and third represent the loss of energy due to friction at the seabed. The power source in (5.1) is the term $RgChvS$ and originates from the acceleration downslope due to gravity.

The dimensional energy equation for the turbulent motion is

$$\frac{\partial}{\partial x}uKh + \frac{\partial}{\partial y}vKh = (P - \epsilon_0)h - RgChv_s - \frac{1}{2}Rghv_s(E_s - C_b) - \frac{1}{2}RgChw_e, \tag{5.3}$$

where K is the turbulence averaged over the vertical and ϵ_0 is the viscous dissipation. This expression originates from consideration of the deviation of the fluid velocity from the mean flow. For the one-dimensional nonrotating case the relation is derived in detail by Parker *et al.* (1986). The two-dimensional equation is derived in Kowalik and Murty (1993) so we do not give the details here. The second term on the right-hand side of (5.3) represents the turbulent energy expended in maintaining the sediment in suspension: the ratio of this term to the power source in (5.1) is the Bagnold-Knapp number $G = v_s/Sv$. The third term represents the loss/gain in turbulent energy due to erosion/deposition. The last term is the loss of turbulent energy due to entrainment. Collectively, the last three terms represent the rate of turbulent energy expenditure due to working against the density gradient. Bagnold (1962) suggested that the condition for 'auto-suspension' or ignition of the current is that $G < 1$ so that there is a surplus of power over that needed to maintain a suspension and the current accelerates downslope. His argument was based purely on energetics and did not include any consideration of sediment exchange so this criterion is not appropriate to the models herein.

To close the model we need to parameterize the entrainment w_e, the viscous dissipation ϵ_0 and the shear velocity $\mathbf{u}_*$. The entrainment is parameterized as in Eq. (2.2) and following Launder and Spalding (1972) we suppose

$$\epsilon_0 = \hat{\gamma}\frac{K^{3/2}}{h}, \tag{5.4}$$

where $\hat{\gamma}$ is a constant determined from the value appropriate for a conservative ($B = G = 0$) gravity current (see later).

We replace the quadratic drag law (2.3) with a relation which supposes the shear stress is some fraction of the turbulence in the plume:

$$(u_*^2, v_*^2) = \hat{\delta}K(1, 1), \tag{5.5}$$

where we initially set $\hat{\delta} = 0.1$ following Parker *et al.* (1986). Some discussion of the merits of this approximation are discussed therein. We are concerned here with the effect such an

assumption has on the qualitative features of the model. One consequence of (5.5) is that erosion is now a function of the turbulence rather than the mean velocity.

Using the scales in Section 2a the nondimensional energy equation for the turbulent motion is

$$(uKh)_x + (vKh)_y = \frac{1}{2}\delta E|\mathbf{U}|^3 + \delta K(u+v) - \frac{\gamma}{\delta^{1/2}}K^{3/2} - \delta GCh - \frac{1}{2}\delta Bk\left(\frac{E_s}{E_{sm}} - C\right)h - \frac{1}{2}\delta EkCh|\mathbf{U}|, \tag{5.6}$$

where the turbulence scale K_* is chosen so that the velocity scale is identical to that in the four-equation model:

$$K_* = \frac{V_*^2}{\delta}, \tag{5.7}$$

and we have introduced the parameters

$$\delta = \frac{\hat{\delta}}{K_f}, \qquad \gamma = \frac{\hat{\gamma}}{K_f}, \qquad G = \frac{v_s}{SV_*}, \qquad k = \frac{K_f}{S}. \tag{5.8}$$

The parameterization of erosion now becomes

$$E_s = E_s(\alpha K^{1/2}), \tag{5.9}$$

where the erosional capacity α is defined as in (2.10). Next we apply the streamtube approximations of Section 3 to yield

$$(AVK)_\xi = \frac{1}{2}\delta EA^{1/2}V^3 + \delta A^{1/2}KV - \frac{\gamma}{\delta^{1/2}}A^{1/2}K^{3/2} - \delta GAC - \frac{1}{2}\delta BkA\left(\frac{E_s}{E_{sm}} - C\right) - \frac{1}{2}\delta EkACV. \tag{5.10}$$

Note that K now represents the turbulence averaged over the cross-section of the tube. The initial turbulence is set so that the tube experiences the same initial frictional force as it did in the four-equation model. This requires we set $K_s = V_s^2$.

To summarize the nondimensional five-equation model is

$$(AV)_\xi = EA^{1/2}V, \tag{5.11a}$$

$$(AVC)_\xi = BA^{1/2}\left(\frac{E_s}{E_{sm}} - C\right), \tag{5.11b}$$

$$(AV^2)_\xi = -A^{1/2}K + AC\sin\beta, \tag{5.11c}$$

$$V^2\beta_\xi = C\cos\beta - \frac{V}{Ro}, \tag{5.11d}$$

$$(AVK)_\xi = \frac{1}{2}\delta E A^{1/2}V^3 + \delta A^{1/2}KV - \frac{\gamma}{\delta^{1/2}}A^{1/2}K^{3/2} - \delta GAC - \frac{1}{2}\delta BkA\left(\frac{E_s}{E_{sm}} - C\right) - \frac{1}{2}\delta EkACV. \tag{5.11e}$$

a. The Kveitehola outflow

The qualitative features of the model are again illustrated with reference to the Kveitehola outflow using the numerical values in Table 1. Following the analysis of the four-equation model (3.8) we look first for uniform solutions. Nonentraining uniform solutions to (5.11) satisfy

$$C_0 = E_s(\alpha K_0^{1/2})/E_{sm}, \tag{5.12a}$$

$$\cos\beta_0 = \frac{V_0}{RoC_0}, \tag{5.12b}$$

$$K_0V_0^{1/2} = C_0\sin\beta_0, \tag{5.12c}$$

$$\delta K_0V_0^{3/2} = \frac{\gamma}{\delta^{1/2}}K_0^{3/2}V_0^{1/2} + \delta GC_0. \tag{5.12d}$$

The value taken for the dissipation γ is chosen so that both the five-equation model and the four equation model give the same uniform solutions for a nonentraining ($E = 0$), conservative ($G = B = 0$) gravity current. This requires that we specify

$$\gamma = \delta^{3/2}. \tag{5.13}$$

After some simplification we find that uniform solutions must satisfy

$$V_0^{5/4} = \left(C_0^2 - \frac{V_0^2}{Ro^2}\right)^{1/4} + \frac{GC_0V_0^{1/4}}{\left(C_0^2 - \frac{V_0^2}{Ro^2}\right)^{1/2}}, \tag{5.14}$$

For $B = G = 0$, $C_0 = C_s$ and we recover Eq. (3.10c) so that the uniform solutions are the same as in the four-equation model. However, for $B \neq 0$ there is a jump in the uniform solutions since then $C_0 = E_s(\alpha K_0^{1/2})/E_{sm}$.

In Figure 7a we plot F_1 and F_2 as functions of K where F_1 and F_2 are given by the left- and right-hand sides of (5.14), respectively. Here we have used the fact that the uniform velocity can be expressed as a function of K_0:

$$V_0 = -\tfrac{1}{2}Ro^2K_0^2 + \tfrac{1}{2}(Ro^4K_0^4 + 4Ro^2C_0^2)^{1/2}. \tag{5.15}$$

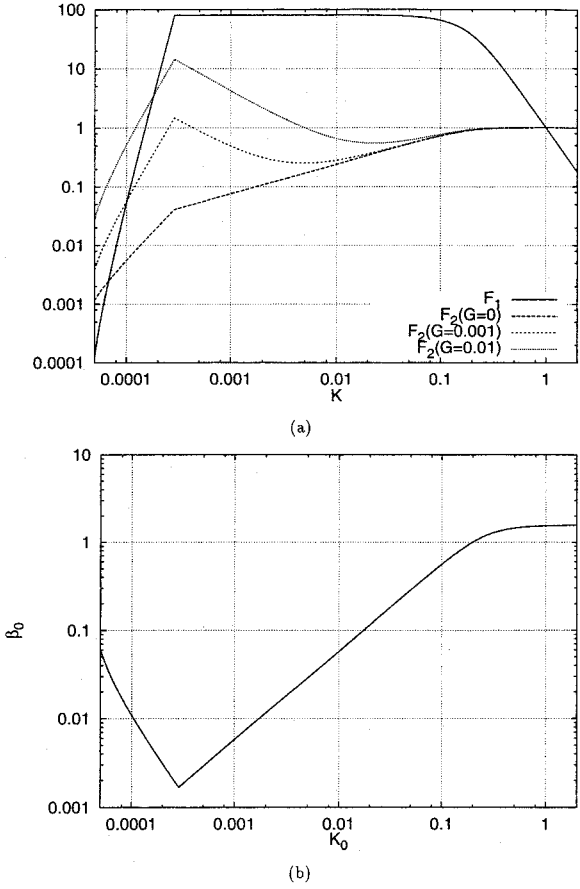

Figure 7. Uniform solutions to the five-equation model with parameters taken from Table 1. (a) shows the uniform solution for a medium silt. There is only one uniform velocity V_0 given by $F_1 = F_2$. (b) shows that this corresponds to two uniform values of K_0.

Thus the uniform solutions K_0 are those values of K at which $F_1 = F_2$. A number of curves of F_2 for increasing values of G are shown. It is clear that there are again two uniform solutions: the left-most root is the geostrophic solution whilst the right-most root $K \sim 1$ is the catastrophic solution. Figure 7b shows β_0 as a function of K_0 and indicates that the geostrophic solution is primarily alongslope while the catastrophic solution is downslope. Increasing G increases the geostrophic uniform turbulence K_0 which corresponds to increasing mean velocity V_0 from (5.15). The catastrophic uniform solutions are unaffected by increasing G since the plume is eroding at the maximum possible rate and the balance is between the first two terms in (5.14).

The values of the geostrophic and catastrophic states of the five-equation model for a medium silt are given in Table 2. The larger geostrophic uniform velocity compared with

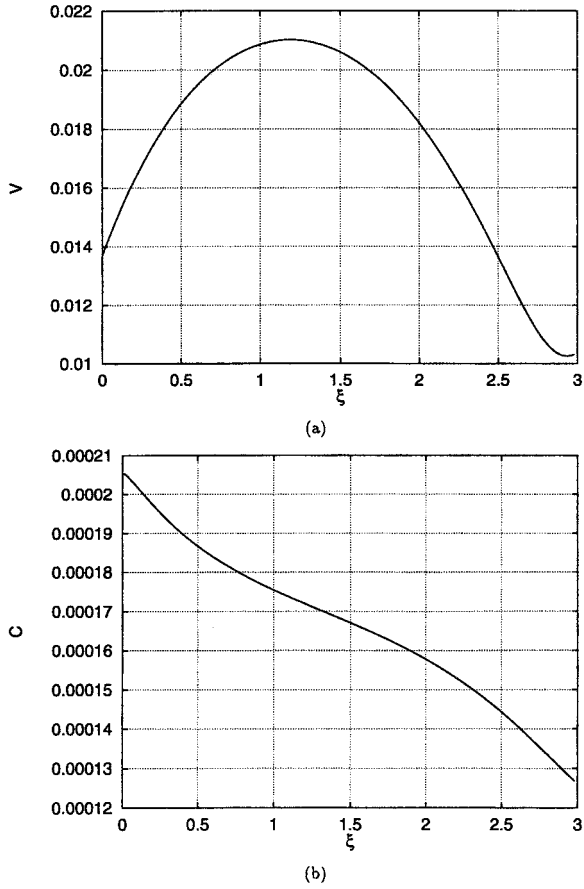

Figure 8. The solution to the five-equation model for a bed containing medium silt. Turbulence dies out in the plume and the model breaks down.

the four-equation model results from the extra energy needed to maintain the sediment in suspension.

Figures 8 and 9 show numerical solutions of (5.11) for a medium and a coarse silt respectively using values in Table 1. We set the entrainment $E = 0$ in order to compare with the four-equation model results.

The medium silt no longer ignites as it did with the four-equation model. Instead the flow is alongslope and the current deposits its load (Fig. 8b). At about 7 km downstream Figure 8d indicates that the turbulence dies out in the plume (the length-scale L is about 2.3 km). At this point the model breaks down since K cannot become negative. In reality the concentration of sediment in the plume will decay exponentially and the turbidity current will be extinguished. The tube containing coarse silt deposits its load as in the four-equation model. From Figure 9b we can see that the current is extinguished at about

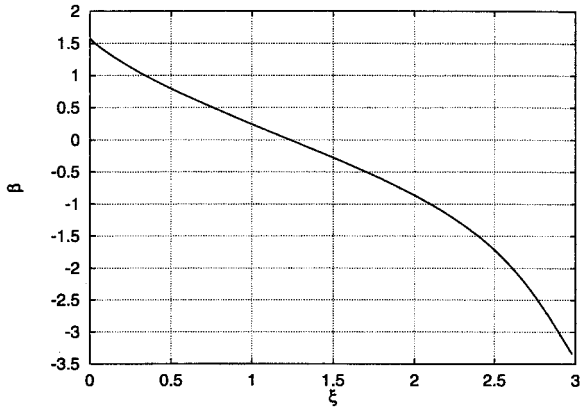

(c)

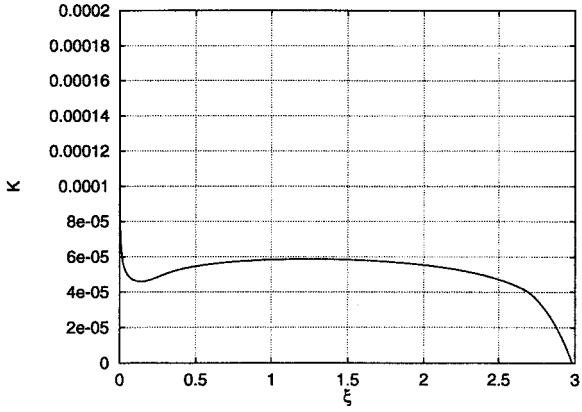

(d)

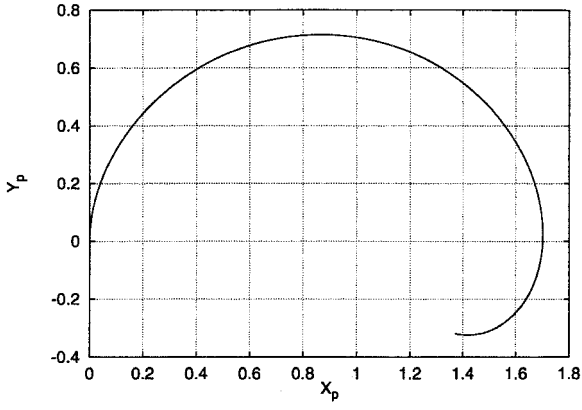

(e)

Figure 8. (Continued)

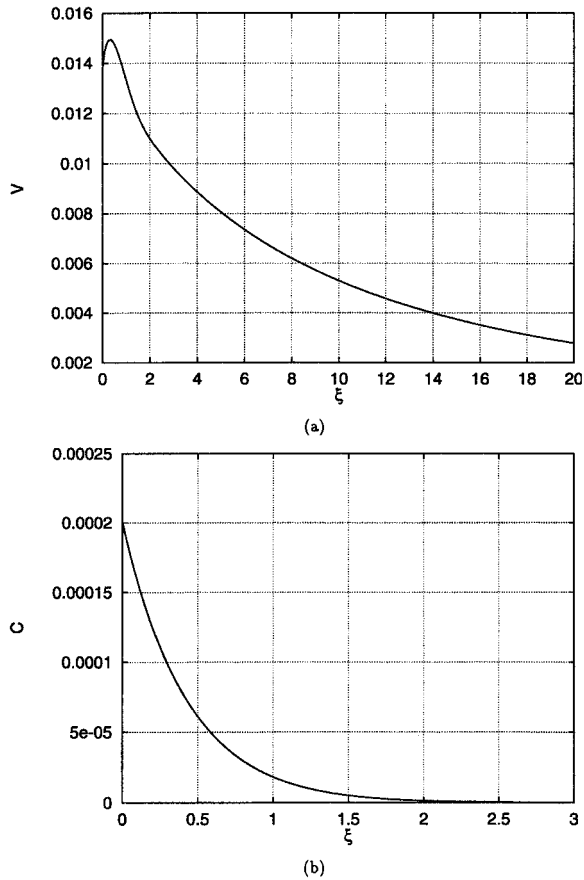

Figure 9. The solution to the five-equation model for a bed containing coarse silt. The tube moves along slope and deposits its load.

7 km downstream as it was with the four-equation model. Figure 9e shows that the tube rapidly circles on the slope and deposits its load about 1.4 km alongslope from the source.

Thus for both example cases the plume deposits its load. However ignition is still possible. If we choose a much smaller value of $\hat{d} = 10^{-4}$ which gives $d = 0.1$ and rerun the model for a medium silt then the solution proceeds to the catastrophic state (Fig. 10). Figure 10e shows the solution igniting about 180 km from the source. However, the tube moves a much larger distance alongslope before ignition really sets in. Figure 8d shows that initially the turbulent energy in the plume is small which means the frictional term in (5.11c) remains small and so the tube moves alongslope. At about $j \sim 80$ the turbulence rapidly increases as more sediment is entrained leading to increasing bottom stress. This then impacts on the mean velocity (Fig. 10a) through the parameterization of bottom friction and the velocity decreases toward the catastrophic value $V \sim 1$.

All the model runs suggest that the geostrophic uniform state is unstable. A linear

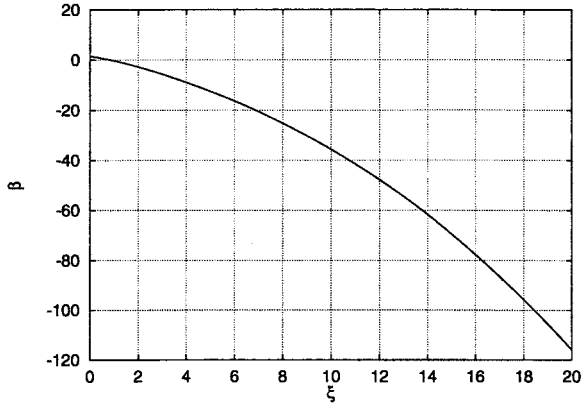

(c)

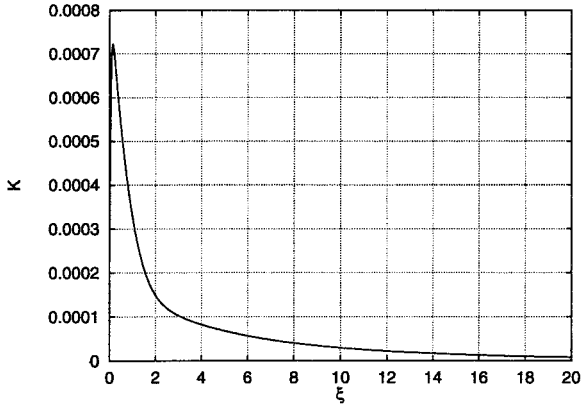

(d)

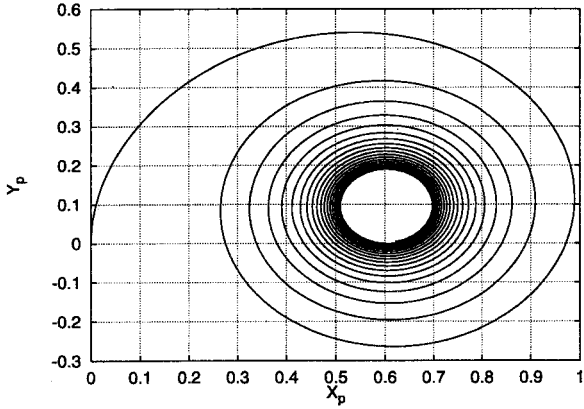

(e)

Figure 9. (Continued)

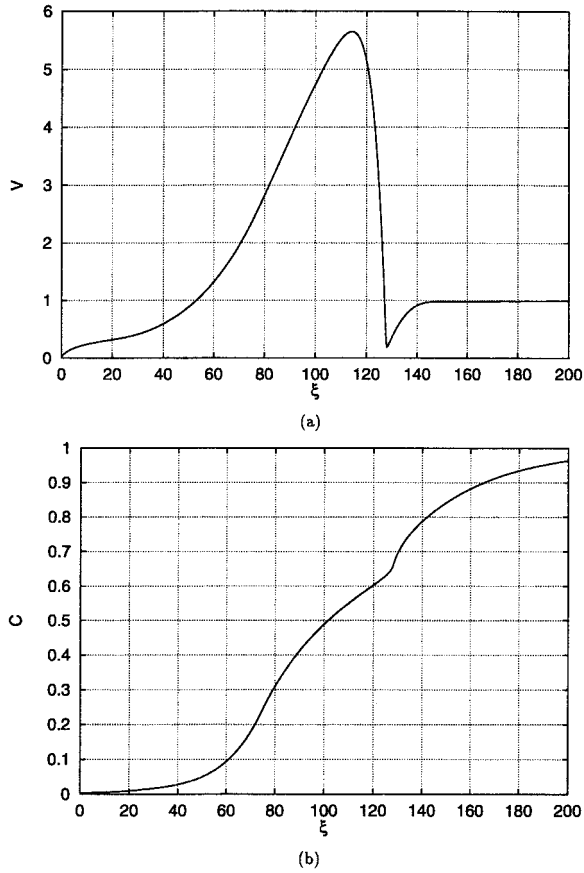

Figure 10. The solution to the five-equation model for a bed containing medium silt and a small shear stress parameter $\delta = 0.1$. The solution proceeds to the catastrophic state.

stability analysis of (5.11) could be performed but now the equation for the eigenvalue will be a quartic and stability could probably only be analyzed numerically.

6. Conclusions

The use of a streamtube model has allowed the prediction of the path a rotating turbidity current takes on a uniform slope. The first model developed is a standard streamtube model with parameterizations for erosion and deposition. This model has two uniform solutions, one of which describes geostrophic alongslope flow while the other describes downslope catastrophic flow. In reality a current in the ocean may never reach such an equilibrium solution: the topography varies along and down the slope. However the linear stability of the uniform states indicates which state the model solution will try to tend toward. It was shown that the geostrophic state is always unstable to perturbations at the source. This means that no matter what initial data we give the model it will never predict flow

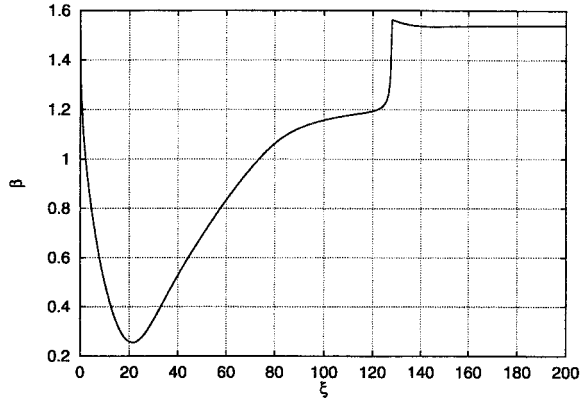

(c)

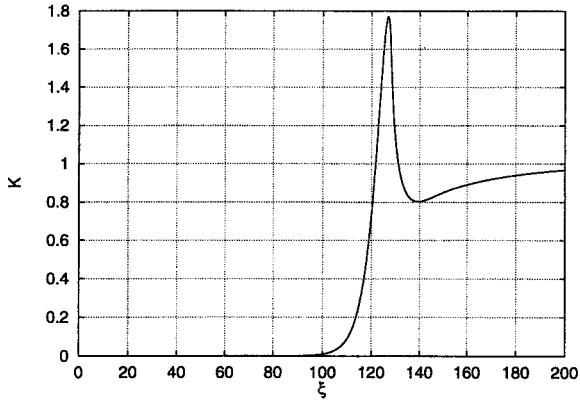

(d)

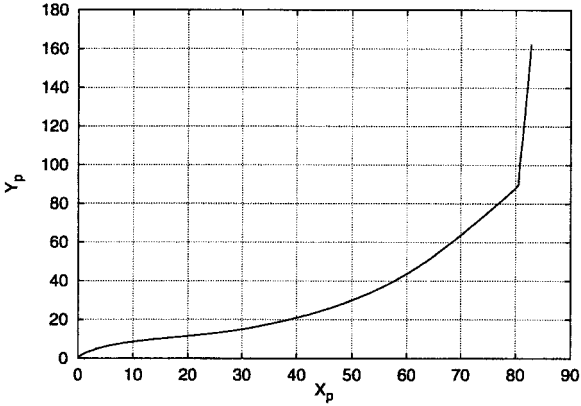

(e)

Figure 10. (Continued)

alongslope. A small perturbation downslope speeds up the flow and so entrains more sediment. The addition this makes to the body force acting downslope far outweighs the addition to the Coriolis force so that flow continues downslope. The catastrophic state was found to be always stable. This means that if we give the model a sufficiently large initial flow velocity it will always proceed to the catastrophic state. Therefore how do we explain the shift to the right of the mean position of the Grand Banks turbidity current if this is an example of an erosive gravity plume?

Parker *et al.* (1986) found the catastrophic state requires more energy to maintain the sediment in suspension than is available to the current. This led us to develop a five-equation model which parameterizes bottom friction based on the turbulence in the plume and includes a turbulent kinetic energy equation. We illustrated the possibilities with reference to the Kveitehola outflow and showed that onset of the catastrophic state was delayed and the tube moved alongslope for many kilometers. Thus the Coriolis force is an important part of the momentum balance in both an erosive plume and a depositional plume. Given the sparsity of experimental and observation data it seems unwise to compute an auto-suspension criterion based on this model especially as the auto-suspension criterion for a nonrotating current is as yet an undecided issue (Stacey and Bowen, 1990). The importance of the Coriolis force on the path of an oceanic turbidity current does seem to be supported by records of cable breakages caused by the Grand Banks turbidity current (Nof, 1996). Numerical models should take account of the turbulent kinetic energy if they are to accurately predict the path of a turbidity current.

The streamtube approximation has been used to derive a simple model. The most drastic assumption in this approximation is that properties across the tube are uniform. For a density-driven current this is not the case. There is some observational evidence in the ocean (Johnson *et al.,* 1994a,b) that an Ekman-like layer exists at the base of the tube which drains the mean flow and seeps downslope. Eventually the drainage of fluid will extinguish the core alongslope flow and the tube will cease to exist after it has traveled a distance $O(Ek^{-1})$ where Ek is the Ekman number. However streamtube models have been successfully applied to a number of oceanic outflows using this assumption (Smith, 1975; Killworth, 1977; Price and Baringer, 1994) and since there is so little data available for turbidity currents it seems a reasonable approximation to make here. One way around this limitation is to consider a fully two-dimensional model with a streamfunction representing the transverse coordinate in the tube. This means that the width no longer need to be parameterized but is part of the solution to the model. However the model equations will now be partial differential equations with free boundaries at the plume edges and consequently will be much more difficult to solve than a streamtube model.

The model derived here assumes that the interstitial water is of the same density as the unstratified ambient water. It is simple to extend the model to include a density contrast. For the case of a depositional plume the behavior after complete deposition depends on the water density difference. If interstitial water is lighter than ambient, then we would expect upwelling (Bennecaze *et al.,* 1993) whereas denser interstitial water would lead to the classical streamtube solution of flow along the slope. Stratification of the ambient water

would favor alongslope flow since moving downslope would decrease the density contrast. However for an ignited turbidity current the dominant driving force is the sediment in the plume and so the effect of stratification in this case is small. If fluid reaches a state of neutral density then the tube circles as it does in Figure 5d.

It is also assumed that there is only one size of sediment in the plume. Again it is simple to extend the streamtube models to consider two types. Larger particles increase the density contrast but also have larger settling velocities so it is not clear how this modification to the model would affect the qualitative results. Current research is aimed at constructing a two-dimensional, two-component version of the model so that the distribution of sediments could be predicted. One might also incorporate a spatial dependence on the available sediment (Fohrmann *et al.,* 1997). This would mean that the erosional parameterization E_s would be a function of position and that the model would be coupled to (3.1).

The rotating streamtube model may also be applied to river outflows, where the suspended sediment is not necessarily driving the flow. Wright *et al.* (1990) examined the deposition of silt from the Huange (Yellow River) and they used a simple streamtube approach to model the undercurrent. The application of more sophisticated models to these outflows is a possible area of future research.

Acknowledgments. This work was supported by the U.K. Natural Environment Research Council Grant GR3/8578. I would like to thank Peter Killworth and Andrew Willmott for their comments and Gregory Lane-Serff for improving the scaling of the equations.

REFERENCES

Akiyama, J. and Y. Fukushima. 1985. Entrainment of noncohesive bed sediment into suspension. External Memo No. 175, St. Anthony Falls Hydraulic Laboratory, University of Minnesota, Minneapolis, USA.

Bagnold, R. A. 1962. Auto-suspension of transported sediment; turbidity currents. Proc. Roy. Soc. Lond. A, *265,* 315–319.

Batchelor, G. K. 1967. An Introduction to Fluid Dynamics, Cambridge University Press, 615 pp.

Bonnecaze, R. T., H. E. Huppert and J. R. Lister. 1993. Particle-driven gravity currents. J. Fluid Mech., *250,* 339–369.

Bouma, A. H., W. R. Normark and N. E. Barnes. (eds). 1985. Submarine Fans and Related Turbidite Systems. New York: Springer-Verlag, 351 pp.

Clarke, J. E. Hughes, A. N. Shor, D. J. W. Piper and L. A. Mayer. 1990. Large-scale current-induced erosion and deposition in the path of the 1929 Grand Banks turbidity current. Sedimentology, *37,* 613–629.

Dade, W. B., J. R. Lister and H. E. Huppert. 1994. Fine-sediment deposition from gravity surges on uniform slopes. J. Sediment. Res., *A64,* 423–432.

Ellison, T. H. and J. S. Turner. 1959. Turbulent entrainment in stratified flows. J. Fluid Mech., *6,* 423–448.

Emms, P. W. 1997. Streamtube models of gravity currents in the ocean. Deep-Sea Res. I, *44,* 1575–1610.

Fohrmann, H., J. O. Backhaus, F. Blaume and J. Rumohr. 1997. Sediments in bottom arrested gravity plumes—Numerical case studies. J. Phys. Oceanogr., (submitted).

Garcia, M. and G. Parker. 1993. Experiments on the entrainment of sediment into suspension by a dense bottom current. J. Geophys. Res., *98(C3),* 4793–4807.

Griffiths, R. W. 1986. Gravity currents in rotating systems. Ann. Rev. Fluid Mech., *18,* 59–89.

Griffiths, R. W., P. D. Killworth and M. E. Stern. 1982. Ageostrophic instability of ocean currents. J. Fluid Mech., *117,* 343–377.

Huppert, H. E., J. S. Turner and M. A. Hallworth. 1995. Sedimentation and entrainment in dense layers of suspended particles stirred by an oscillating grid. J. Fluid Mech., *289,* 263–293.

Johnson, G. C., T. B. Sanford and M. Baringer. 1994a. Stress on the Mediterranean outflow plume: Part I. Velocity and water property measurements. J. Phys. Oceanogr., *24,* 2072–2083.

Johnson, G. C., R. G. Lueck and T. B. Sanford. 1994b. Stress on the Mediterranean outflow plume: Part II. Turbulent dissipation and shear flow measurements. J. Phys. Oceanogr., *24,* 2084–2092.

Junghaus, J. H. and J. O. Backhaus. 1994. Application of a transient reduced gravity plume model to the Denmark Strait Overflow. J. Geophys. Res., *99(C6),* 12,375–12,396.

Killworth, P. D. 1977. Mixing on the Weddell Sea continental slope. Deep-Sea Res., *24,* 427–448.

Kowalik, Z. and T. S. Murty. 1993. Numerical modeling of ocean dynamics. Advanced Series on Ocean Engineering, *5,* World Scientific, 480 pp.

Launder, B. E. and D. B. Spalding. 1972. Mathematical Models of Turbulence, Academic, 169 pp.

Nof, D. 1996. Rotational turbidity flows and the 1929 Grand-Banks earthquake. Deep-Sea Res., *43,* 1143–1163.

Pantin, H. M. 1979. Interaction between velocity and effective density in turbidity flow: phase-plane analysis, with criteria for autosuspension. Mar. Geol., *31,* 59–99.

Parker, G. 1982. Conditions for the ignition of catastrophically erosive turbudity currents. Mar. Geol., *46,* 307–327.

Parker, G., Y. Fukushima and H. M. Pantin. 1986. Self-accelerating turbidity currents. J. Fluid Mech., *171,* 145–181.

Piper, D. J. W. and B. Savoye. 1993. Processes of late Quaternary turbidity current flow and deposition on the Var deep-sea fan, north-west Mediterranean Sea. Sedimentology, *40,* 557–582.

Price, J. F. and M. Baringer. 1994. Outflows and deep water production by marginal seas. Prog. Oceanog., *33,* 161–200.

Rimoldi, B., J. Alexander and S. Morris. 1996. Experimental turbidity currents entering density-stratified water: analogues for turbidities in the Mediterranean hypersaline basins. Sedimentology, *43,* 527–540.

Smith, P. C. 1973. The dynamics of bottom boundary currents in the ocean. Ph.D. thesis, Massachusetts Institute of Technology, 214 pp.

—— 1975. A streamtube model for the bottom boundary currents in the ocean. Deep-Sea Res., *22,* 853–874.

Stacey, M. W. and A. J. Bowen. 1990. A comparison of an autosuspension criterion to field observations of five turbidity currents. Sedimentology, *37,* 1–5.

Stow, D. A. V. 1994. Deep Sea processes of sediment transport and deposition, *in* Sediment Transport and Depositional Processes, K. Rye, ed., Blackwell Sci. Publ., 257–291.

Swaters, G. E. 1991. On the baroclinic instability of cold-core coupled density fronts on a sloping continental shelf. J.Fluid Mech., *224,* 361–382.

Swaters, G. E. and G. R. Flierl. 1991. Dynamics of ventilated coherent cold eddies on a sloping bottom. J. Fluid Mech., *223,* 565–587.

Turner, J. S. 1986. Turbulent entrainment: the development of the entrainment assumption, and its application to geophysical flows. J. Fluid Mech., *173,* 431–471.

Wright, L. D., Jr, W. J. Wiseman, Z. S. Yang, B. D. Bornhold, G. H. Keller, D. B. Prior and J. N. Suhayda. 1990. Processes of marine dispersal and deposition of suspended silts off the modern mouth of the Huanghe (Yellow River). Cont. Shelf Res., *10,* 1–40.

Received: *28 May, 1997;* revised: *30 September, 1997.*